Spectrum Sensing With High Sensitivity and Interferer Robustness Using Cross-Correlation Energy Detection

Mark S. Oude Alink, *Student Member, IEEE*, André B. J. Kokkeler, Eric A. M. Klumperink, *Senior Member, IEEE*, Gerard J. M. Smit, and Bram Nauta, *Fellow, IEEE*

***Abstract*—Dynamic spectrum access relying on spectrum sensing requires reliable detection of signals in negative signal-to-noise ratio (SNR) conditions to prevent harmful interference to licensed users. Energy detection (ED) is a quite general solution, which does not require any knowledge of the signals to be detected. Unfortunately, it suffers from noise uncertainty in the receiver, which results in an SNR-wall below which signals cannot be reliably detected. Furthermore, distortion components originating from nonlinearity in the sensing receiver cannot be distinguished from true input signals, and is thus another effect that may obscure weak signals and cause false alarms or missed detections. Cross-correlation was recently proposed to reduce the SNR-wall and, at the same time, allow the receiver to be designed for high linearity. This allows for high-fidelity spectrum sensing, both in the presence of strong interference as well as for signals with a negative SNR. In this work, an integrated complementary metal–oxide–semiconductor prototype exploiting cross correlation is presented and tested in practice. The prototype achieves a high linearity of $+25$ dBm IIP3 at a sensitivity of -184 dBm/Hz, 10 dB below the kT noise floor. The measured results agree well with theory, and, compared to the traditional ED-approach, show both a significant improvement in sensing time, as well as a reduction of 12 dB in the SNR-wall itself. Overall, cross-correlation makes ED faster, more sensitive, more resilient to strong interferers, and more energy-efficient.**

***Index Terms*—Cognitive radio, cross-correlation, dynamic spectrum access, energy detection, experimental verification, IIP3, linearity, measurements, noise uncertainty, radiometer, sensitivity, spurious-free dynamic range (SFDR), signal detection, signal-to-noise ratio (SNR)-wall, spectrum sensing.**

I. Introduction

DYNAMIC spectrum access with a cognitive radio is a promising paradigm to improve the efficiency of spectrum use. Unlicensed users, or secondary users, opportunistically use spectrum that is temporarily and locally unused by the licensed user, the primary user. The process of how to identify this unoccupied spectrum, which is also known as "white space," is an ongoing debate.

Field trials conducted by the Federal Communications Commission (FCC) in 2008 showed that the prototypes provided by industrial players were able to reliably detect very weak signals in an otherwise clean spectrum, but failed in the presence of a strong interferer [1]. Based on these results and several public discussions, the FCC came with a new publication in 2010 [2], favoring a database approach with location and channel availability information over spectrum sensing. It states: *"Our actions here are expected to spur investment and innovation in applications and devices that will be used not only in the TV band but eventually in other frequency bands as well."* The FCC decided that *"eliminating the requirement that TV bands devices that incorporate geo-location and database access must also listen (sense) to detect the signals of TV stations and low power auxiliary service stations"* was the best way to go forward.

Although spectrum sensing in TV white space has thus become unnecessary, regulations for spectrum-sensing-only devices are still included, because *"we are encouraging continued development of [spectrum sensing] because we believe it holds promise to further improvements in spectrum efficiency in the TV spectrum in the future and will be a vital tool for providing opportunistic access to other spectrum bands"* [2]. Sensing will be necessary for (ad-hoc) networks of dynamic spectrum access devices that lack infrastructure, or where a central database is rendered useless due to the fast rate of change in the spectrum usage. Furthermore, a spectrum sensing capability is useful for the classification of white spaces in terms of receiver requirements (filtering, nonlinearity, etc.) based on current local spectrum conditions [3], for determining the desired rejection frequency of a tunable notch filter [4], and for monitoring the transmitter output spectrum for on-the-fly tuning of digital predistortion and spur reduction [5], [6].

The prototypes discussed in [1] most likely failed in the presence of a large interferer due to their inability to simultaneously detect strong and weak signals. Recently, we presented cross-correlation (XC) as a solution [7]–[10], and theoretically hypothesized it to be more sensitive (reduced signal-to-noise ratio (SNR)-wall [8]) and robust for interference (high spurious-free dynamic range (SFDR) [7], [9]). This paper presents the first measurement results that actually demonstrate the improvement in sensitivity (reduced SNR-wall). Moreover, this paper reviews previous work and highlights the key reasons for high SFDR, and analyzes the trade-off between SFDR and measurement time.

Manuscript received April 20, 2013; revised July 04, 2013; accepted July 20, 2013. Date of publication September 24, 2013; date of current version December 09, 2013. This paper was recommended by Guest Editor R. Gomez-Garcia.

M. S. Oude Alink was with the Computer Architecture for Embedded Systems Group and the IC-Design Group, Centre for Telematics and Information Technology, University of Twente, 7500 AE Enschede, The Netherlands. He is now with Bruco Integrated Circuits, 7623 CS Borne, The Netherlands (e-mail: mark.oude.alink@bruco.nl).

A. B. J. Kokkeler and G. J. M. Smit are with the Computer Architecture for Embedded Systems Group, Centre for Telematics and Information Technology, University of Twente, 7500 AE Enschede, The Netherlands.

E. A. M. Klumperink and B. Nauta are with the IC-Design Group, Centre for Telematics and Information Technology, University of Twente, 7500 AE Enschede, The Netherlands.

Color versions of one or more of the figures in this paper are available online at http://ieeexplore.ieee.org.

Digital Object Identifier 10.1109/JETCAS.2013.2280809

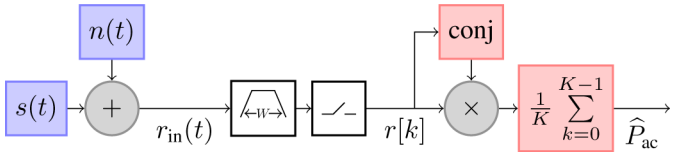

Fig. 1. ED using AC.

The structure of this paper is as follows. In Section II, energy detection (ED) and the influence of circuit nonidealities on the performance are discussed. The XC technique, which is a form of ED, is summarized in Section III, together with its benefits for spectrum sensing performance and system design. A prototype to demonstrate these benefits was implemented in 65 nm complementary metal–oxide–semiconductor (CMOS) technology; its design is summarized in Section IV, together with measurement results showing its high SFDR. The main contribution of this paper is the experimental verification of the theoretical hypothesis that XC has better sensing performance than standard ED in terms of speed, sensitivity, and energy consumption. These measurements are described in detail in Section V. We end with conclusions in Section VI.

II. Energy Detection and Circuit Nonidealities

Different spectrum sensing techniques exist, but one of the most promising in terms of general applicability is ED, which does not rely on any knowledge of the signals to be detected, and can thus be used anywhere in any band. It measures the power (or energy) in a frequency band to decide whether a signal is present or not.

If the receiver/energy detector is modeled as a device that only adds noise, and the bandwidth is sampled at the Nyquist rate, the result is a complex baseband receiver output $r[k]$. The detector has to decide which of the following two hypotheses is true:

$$\begin{aligned} \mathcal{H}_0 &: r[k] = n[k] \qquad \text{(only noise)} \\ \mathcal{H}_1 &: r[k] = s[k] + n[k] \qquad \text{(signal plus noise).} \end{aligned} \tag{1}$$

First, the output power is estimated as $\widehat{P}$ using K (independent) complex samples, with $\widehat{P}$ some function of r. For autocorrelation (AC), which is taken here as the standard form of ED, the subscript "ac" is used. $\widehat{P}$ for AC, as shown in Fig. 1, is

$$\widehat{P}_{\text{ac}} = \frac{1}{K} \sum_{k=0}^{K-1} |r[k]|^2. \tag{2}$$

The problem now is to set a threshold λ such that

$$\begin{aligned} P_{\text{FA}} &\triangleq \mathbb{P}\left(\widehat{P} > \lambda | \mathcal{H}_0\right) \leq P_{\text{FA,des}} \\ P_{\text{MD}} &\triangleq \mathbb{P}\left(\widehat{P} < \lambda | \mathcal{H}_1\right) \leq P_{\text{MD,des}} \end{aligned} \tag{3}$$

with $\mathbb{P}(\cdot|\cdot)$ a conditional probability, P_{FA} and P_{MD} the probabilities of false alarm and missed detection, and the subscript "des" indicating desired (upperbound) values. Since the power of the signal is not known *a priori*, one usually determines λ by setting P_{FA} equal to $P_{\text{FA,des}}$. With K large enough to justify Gaussian approximations, one can find

$$P_{\text{FA}} \approx Q\left(\frac{\lambda - \mu_0}{\sigma_0}\right) \qquad P_{\text{D}} \approx Q\left(\frac{\lambda - \mu_1}{\sigma_1}\right) \tag{4}$$

with P_{D} the probability of detection ($P_{\text{D}} \triangleq 1 - P_{\text{MD}}$), and μ_0 (μ_1) the mean and ${\sigma_0}^2$ (${\sigma_1}^2$) the variance of $\widehat{P}$ for $\mathcal{H}_0$ ($\mathcal{H}_1$).

For $\widehat{P}_{\text{ac}}$, these two moments are [11]

$$\mu_{\text{ac}} \approx 1 + \text{SNR} \qquad \sigma_{\text{ac}} \approx \frac{\sqrt{1 + 2\text{SNR}}}{\sqrt{K}}. \tag{5}$$

This implies that for $K \to \infty$, $P_{\text{FA}} \downarrow 0$ and $P_{\text{D}} \uparrow 1$.

A. Noise Uncertainty

The decision threshold λ is based on the noise power level, which is composed of noise from the physical channel and noise from the receiving device, the latter of which usually dominates. The noise level needs to be estimated, and is only known to within a certain accuracy, e.g., due to the fact that the noise of the receiver may vary over frequency and during operation, and the noise level estimation itself will always have some error [11]–[13]. Phase noise also adds to the noise uncertainty, because its impact depends on current spectrum conditions. This is because it manifests itself mostly around strong input signals via reciprocal mixing.

When the noise power is estimated, with $(1-\epsilon_1){\sigma_n}^2 \leq \widehat{\sigma}_n^2 \leq (1+\epsilon_2){\sigma_n}^2$, where $0 \leq \epsilon_1 < 1$ and $\epsilon_2 \geq 0$, one can define a peak-to-peak uncertainty U as [11]

$$U \triangleq \frac{1+\epsilon_2}{1-\epsilon_1} \tag{6}$$

such that a threshold to guarantee both inequalities in (3) is

$$\lambda_{\text{ac}} = U\left(\mu_{\text{ac},0} + \sigma_{\text{ac},0} Q^{-1}\left(P_{\text{FA,des}}\right)\right). \tag{7}$$

The subscript "0" indicates the statistics are based on $\mathcal{H}_0$. Solving this for given K, $P_{\text{FA,des}}$, and $P_{\text{D,des}}$, the minimum SNR that can be robustly detected is limited by U [11]

$$\text{SNR}_{\text{min,ac}} = (U-1) + \mathcal{O}\left(\frac{1}{\sqrt{K}}\right). \tag{8}$$

Thus, ED cannot detect signals below a certain SNR, the SNR-wall, which is why many implementations choose to exploit known features of the signals to be detected, see e.g., [14].

B. Nonlinearity

To analyze nonlinearity effects of receivers, their output can usually be reasonably well described by (neglecting noise, frequency translation, and filtering) $r(t) \approx a_1 s(t) + a_2 s^2(t) + a_3 s^3(t)$. The coefficients a_2 and a_3 distort the spectrum; a_3 usually dominates. If sine waves at frequencies f_1 and f_2 are applied to the system input, a_3 generates components at $2f_1 - f_2$ and $2f_2 - f_1$. The input-referred third-order intermodulation intercept point (IIP3) is the (extrapolated) input power (usually expressed in dBm) for which these distortion products have the same power as the desired components. Like phase noise, these distortion components may be considered as additional noise,

or perhaps better in the context of signal detection, *additional noise uncertainty*. Note that the same thing can be said for other nonideal effects such as downconversion of signals and noise from higher harmonics of the local oscillator (LO).

The FCC requires signals down to $-114\,\mathrm{dBm}$ (in $6\,\mathrm{MHz}$ bandwidth) to be detected [14], so the distortion products should be smaller than that. If f_1 and f_2 are close to the channel that is being sensed, it is very difficult to filter them out. Considering that signals above $-25\,\mathrm{dBm}$ may be received [15], this requires IIP3 $> +20\,\mathrm{dBm}$, while state-of-the-art CMOS receiver IIP3 is in the range of $-20\,\mathrm{dBm}$ to $10\,\mathrm{dBm}$, see Table I. Since a completely integrated solution requires some variable gain, it is hard to directly compare noise figure (NF) and IIP3: the change in NF and IIP3 depends on where the gain is changed. Nevertheless, these numbers show that no implementation comes even close to the required $+20\,\mathrm{dBm}$.

C. Spurious-Free Dynamic Range

For faster spectrum sensing, one would like to sense multiple channels at once. White space may be located just next to a very strong signal, so the (SA) should have both a high linearity and a low NF. A low-noise amplifier (LNA) can ensure low NF, but the amplified signals create distortion products. An attenuator can improve linearity, but at the cost of NF.

The SFDR defines the difference in decibels between the strongest and weakest signal that can be detected *at the same time* [24].[1] Thus, the SA requires a high SFDR. The SFDR is limited by nonlinearity and noise, but also by any spurious components ("spurs"), e.g., from the phase-locked loop (PLL) or from harmonic downmixing. If the spurs can be reduced to negligible levels, and IIP3 is the limiting linearity factor, the following equation for SFDR can be derived [24], [25]:

$$\mathrm{SFDR} = \frac{2}{3}\left(\mathrm{IIP3} - \mathrm{NF} - 10\log_{10}\mathrm{RBW} + 174\right)\ [\mathrm{dB}]. \quad (9)$$

A lower resolution bandwidth (RBW) means that less noise power will be present in such a band, and hence the SFDR increases. The useful increase in SFDR by lowering RBW is limited by the bandwidth of the signals to be detected; at some point, the signal power will also drop, such that the SNR is not further increased when RBW is lowered. Equation (9) assumes that the input signal can be attenuated or amplified to a level where the intermodulation components are at the same level as the noise floor. The SFDR calculated from NF and IIP3 in $1\,\mathrm{MHz}$ RBW is also shown in Table I.

The balancing of noise and intermodulation products is illustrated in Fig. 2. Here it is assumed that the gain control is implemented by an attenuator at the input of the SA (CMOS-attenuators can achieve IIP3 $\gg +30\,\mathrm{dBm}$ [26]). When the linearity is limited by the LNA, it can only be improved by attenuating the signal in front of the LNA. Assuming a matched system and an ideal attenuator, x dB of attenuation raises both NF and IIP3 by x dB. At the input of the SA (top-left), six sine waves are present (circles indicate their power levels for easy reference). At the output, the spectrum looks quite different and depends on the attenuation (the power levels are referred to the antenna). At low attenuation (bottom-left), the strongest signals generate many intermodulation products, which may generate false alarms. At high attenuation (top-right), the increased noise obscures weak signals, which may generate missed detections. Even at the optimum attenuation (bottom-right; 29 dB here) where the noise and distortion products are at the same level and the SFDR of (9) is obtained, some signals cannot be detected.

[1]Definitions of SFDR differ between fields and even between authors in the same field. Here the definition for the SFDR in SA-datasheets is used.

TABLE I
WIDEBAND CMOS-RECEIVER PERFORMANCE OVERVIEW

Reference	Node [nm]	RF Freq. [GHz]	Power [mW]	Gain [dB]	NF [dB]	*In-band* IIP3 [dBm]	SFDR (1 MHz RBW) [dB]
Soer [16]	65	0.2–2.0	67	19	6	11	79
Ru [17]	65	0.4–0.9	60	34	4	4	76
Cai [18]	130	1.0–10	21	20	5	0	73
Blaakmeer [19]	65	0.5–7.0	16	18	5	-3	71
Leenaerts [20]	65	3.0–9.0	156	56	5	-4	70
Greenberg [21]	80	0.04–1.0	440		3	-15	64
Murphy [22]	40	0.08–2.7	78	70	2	-22	60
Youssef [23]	65	0.1–2.5	62	30	8	-20	57

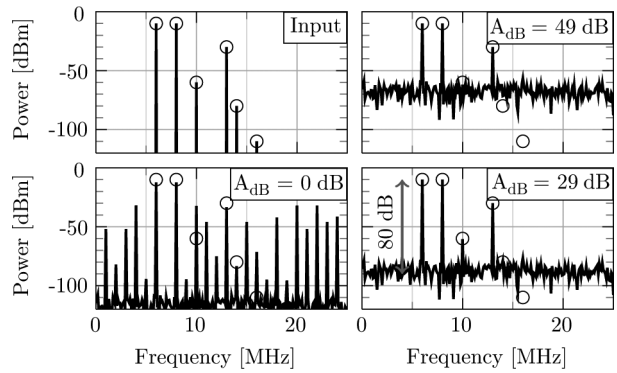

Fig. 2. Simulation of a SA with NF=5 dB and IIP3=+1 dBm. RBW is 100 kHz for a SFDR of 80 dB. Due to noise and distortion products (i.e., limited SFDR), it is not possible to detect all input signals at the same time.

III. CROSS-CORRELATION

In [8], XC is proposed to mitigate the noise uncertainty problem for ED, achieve a higher receiver linearity, and speed up the sensing time. As shown in Fig. 3, rather than conjugating and squaring the output of a single receiver, the outputs of the two receivers are multiplied (with one receiver output conjugated). As a result, the input signal undergoes AC (which can thus be used to obtain its spectrum), while the noise contributions of the individual receivers are cross-correlated and largely average out.

For fair comparison with AC (Fig. 1), define ${\sigma_n}^2 = {\sigma_{n_0}}^2 + {\sigma_{n_1}}^2 = {\sigma_{n_0}}^2 + {\sigma_{n_2}}^2$, such that the SNR at the receiver outputs is the same. Define ${\sigma_{n_0}}^2 = \rho{\sigma_n}^2$, such that ρ denotes the noise correlation between the two receivers, referred back to n_0. As power estimator can be used (subscript "xc" for XC) [8]

$$\widetilde{P}_{\mathrm{xc}} \triangleq \left|\widehat{P}_{\mathrm{xc}}\right| = \left|\frac{1}{K}\sum_{k=0}^{K-1} r_1[k]\overline{r_2[k]}\right|. \quad (10)$$

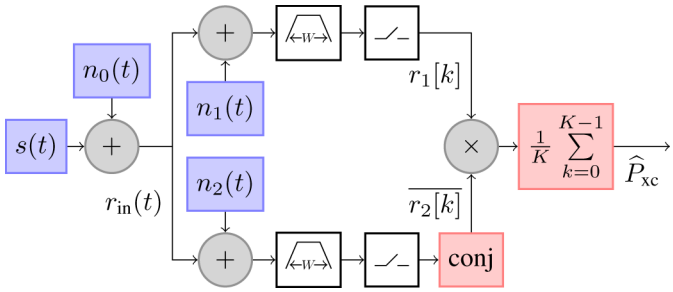

Fig. 3. XC is a generalization of AC (see Fig. 1).

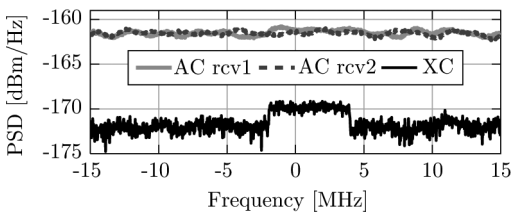

Fig. 4. Visual example of the benefit of XC with respect to AC in the presence of noise uncertainty.

With K large enough to justify Gaussian approximations [8]

$$\mu_{\text{xc}} \approx \sqrt{(\text{SNR}+\rho)^2 + \frac{\beta}{K}((1-\rho^2)+2(1-\rho)\text{SNR})}$$
$$\sigma_{\text{xc}} \approx \frac{\sqrt{\text{SNR}^2 + (2-2\beta+2\beta\rho)\text{SNR} + 1 - \beta + \beta\rho^2}}{\sqrt{K}} \tag{11}$$

where β is an interpolation function, defined as

$$\beta \triangleq \frac{1}{2}\zeta + \frac{\pi}{4K}\left(\frac{\Gamma\left(K+\frac{1}{2}\right)}{\Gamma(K)}\right)^2 (1-\zeta)$$
$$\zeta \triangleq \frac{K\left(\rho+SNR\right)^2}{\text{SNR}\left(K+3-2\rho\right)+\rho\left(K+1-\rho\right)+1} \tag{12}$$

with $\Gamma(\cdot)$ the mathematical Gamma-function. The same derivation using U then results in [8]

$$\text{SNR}_{\text{min,xc}} = \rho(U-1) + \mathcal{O}\left(\frac{1}{\sqrt{K}}\right). \tag{13}$$

Note that XC is equal to AC when $\rho = 1$. Clearly, a lower ρ should result in a lower SNR-wall.

The improvement of XC as compared to AC is illustrated in Fig. 4, where the noise uncertainty is modeled as a nonwhite noise floor. The AC-spectra of the individual receivers show no signal, while it clearly pops up in the XC-spectrum.

An input attenuation of 3 dB improves IIP3 by 3 dB, but also increases noise by 3 dB. If the signal is attenuated after the signal is split between the two receivers, rather than directly after the antenna, the absolute signal power at the antenna input that can be detected remains the same [9]. This is due to the fact that the noise added by the attenuators only adds to n_1 and n_2 in Fig. 3, and not to n_0. With XC, the noise floor can be reduced by 3 dB by increasing the measurement time by a factor 4 [both the mean and the standard deviation of the estimator scale with $\sqrt{K}$, see (11)]. Thus, XC allows receivers to have a higher linearity by input attenuation without sacrificing sensitivity, but at the cost of measurement time. Fig. 5 shows this trade-off in a graphical way, for IIP3 as well as SFDR. Note that an improvement of 3 dB in IIP3 gives 2 dB improvement in SFDR, see (9).

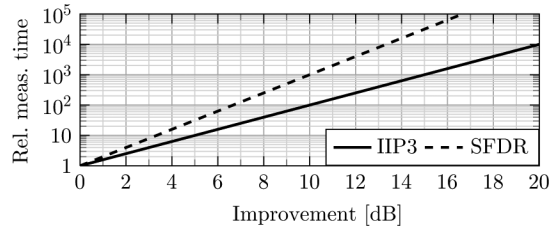

Fig. 5. Trade-off for XC between improved linearity and SFDR (assuming input attenuation) on the one hand and measurement time to keep the same sensitivity on the other hand.

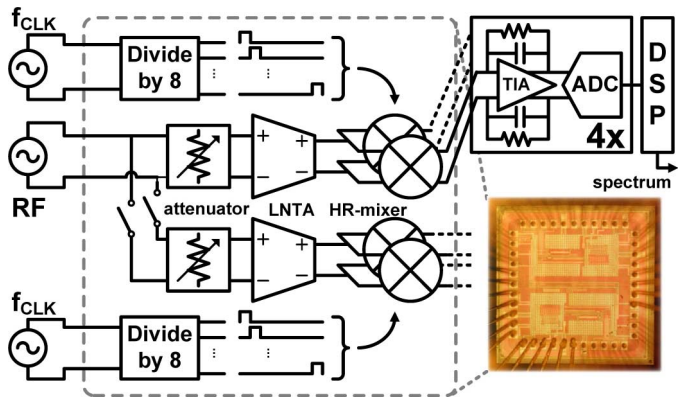

Fig. 6. System setup and chip photo (integrated parts inside dashed box).

Like thermal noise, phase noise can be reduced via the same process at the same time if (part of) the phase noise of the LOs in each receiver is uncorrelated [9], [10], which seems possible. As shown in [27], harmonic rejection (HR) can be improved via XC as well, although it requires a different LO-frequency in each receiver. The use of different LO-frequencies introduces crosstalk in this prototype [27], [28].

Correlated noise due to e.g., the power supply or crosstalk will increase ρ. If this increase is not well known or cannot be measured well, it may equivalently be modeled by an increase in the noise uncertainty U (note that in our model, U is assumed to be the same for both correlated and uncorrelated noise). In both cases, the sensing performance is degraded by the same amount.

IV. Prototype Implementation

To verify the performance of XC experimentally, two RF-frontends are integrated on a single 65 nm CMOS chip. The baseband circuitry and analog-to-digital converters (ADCs) are left off-chip, and the signal processing is performed on a PC. The whole system is shown in Fig. 6.

The frontends can be used separately (e.g., for regular reception), or can be put in parallel via on-chip switches to enable XC spectrum sensing. In this mode, both receivers switch to 100 Ω input impedance mode (assumed throughout this paper), as is more elaborately described in [10]. Each frontend consists

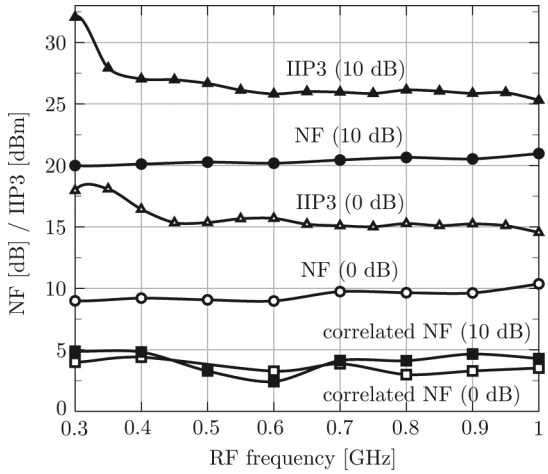

Fig. 7. Performance summary of the prototype.

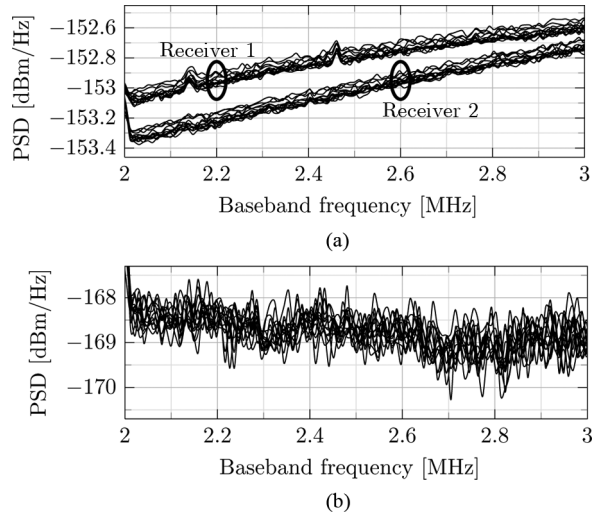

Fig. 8. Measured noise floor between 2 MHz and 3 MHz at different points in time during the measurements. (a) Individual receivers ($K = 1.35 \cdot 10^6$). (b) After XC ($K = 1.35 \cdot 10^6$).

of a discrete-step attenuator, low-noise transconductance amplifier (LNTA), and HR-mixer. The discrete-step attenuator at the inputs of the receivers can provide up to 10 dB attenuation to improve linearity, but at the cost of NF. These attenuators use an IM3-distortion-cancellation technique as described in [26] in order not to limit overall linearity. The LNTAs are designed for high linearity by using a CG-CS topology, similar to [17], and achieve +16 dBm IIP3. The HR-mixers are passive and are sized not to limit overall linearity. The external transimpedance amplifiers (TIAs) convert the output current to a voltage, which is then sampled by the ADCs for further processing.

Some frontend performance parameters without and with the 10 dB attenuation are shown in Fig. 7 (indicated with "(0 dB)" and "(10 dB)," respectively). The power consumption is around 50 mW; more results can be found in [10].

The high in-band IIP3 of +15 dBm allows the system to cope with strong input signals without creating significant distortion and thus false alarms. The noise performance, however, is rather poor at a NF of 10 dB. At 10 dB attenuation, NF and IIP3 increase by 10 dB. The correlated noise floor (obtained after XC) remains the same, as was predicted in [9].

V. SNR-Wall Measurements

By processing the output of a single receiver, the estimators $\widehat{P}_{\rm ac}$ and $\widetilde{P}_{\rm xc}$ can be directly compared: the samples, and thus any temperature and gain variations, are identical. Based on the measurement results of the prototype, the frequency is chosen at 400 MHz, where there is good input matching. To obtain IIP3 well above the desired +20 dBm, the 10 dB attenuation setting is used in all measurements.

A higher linearity reduces intermodulation products. Therefore, a higher linearity makes a spectrum sensing device more robust to strong interference. Unfortunately, it is not possible in our current setup to measure the sensing performance in the presence of interferers. The external ADCs we use suffer from a large amount of correlated noise (probably a common noisy sampling clock generation and common interference from other electronics inside the PC) [27]. To reduce the input-referred correlated noise due to these ADCs, and thereby their negative effect on the sensing performance, the IF-circuitry provides a lot of gain. Any interferer, significant enough to cause some intermodulation, then causes the ADCs to clip. Future work should use different ADCs or integrate them to enable those measurements.

A. Measurement Procedure

The measurement process involves a number of steps.

1) Measure the noise floor and peak-to-peak uncertainty.
2) Find $\lambda_{\rm ac}$ and $\lambda_{\rm xc}$ ($P_{\rm FA,des} = 0.1$) for various K and SNR.
3) Determine the output SNR for a given input power.
4) Find $P_{\rm D}$ for various K and SNR using λ from step 2.

These steps will now be explained in more detail.

The noise floor is determined by measuring the averaged output spectrum of the individual receivers and that obtained with XC without applying an input signal.[2] The ADCs sample at 10 MS/s: the baseband frequency ranges from −5 MHz to 5 MHz. In every measurement, 1024-pt fast Fourier transforms (FFTs) with rectangular windows are used (verifications with other FFT-sizes give similar results). The noise power is determined by adding the power in the 103 bins that have a center frequency between 2 MHz and 3 MHz. The first measurement was started about an hour after turning on all equipment to allow everything to reach thermal equilibrium.

Fig. 8 shows the output noise floors of 13 measurements, performed at the start, at the end, and in between measurements with a signal present. The last measurement was done almost two hours after the first measurement. Clearly, the noise level fluctuates over time, which was also observed in [12]. The difference between the highest and lowest total power in these bands is an indication of the peak-to-peak uncertainty U. The origin of the small peaks that can be observed in the spectrum of receiver 1 at 2, 2.15, and 2.45 MHz is unknown, but unlikely

[2]When used in practice, it is not known whether there is an input signal or not. This makes it much harder or perhaps even impossible to estimate the noise floor at run-time [13]. Factory calibration, similar to what is done here, or (periodic) calibration by switching out the antenna and terminating the receiver input with a 50 Ω resistor may be alternative options. This problem is not further explored in this work.

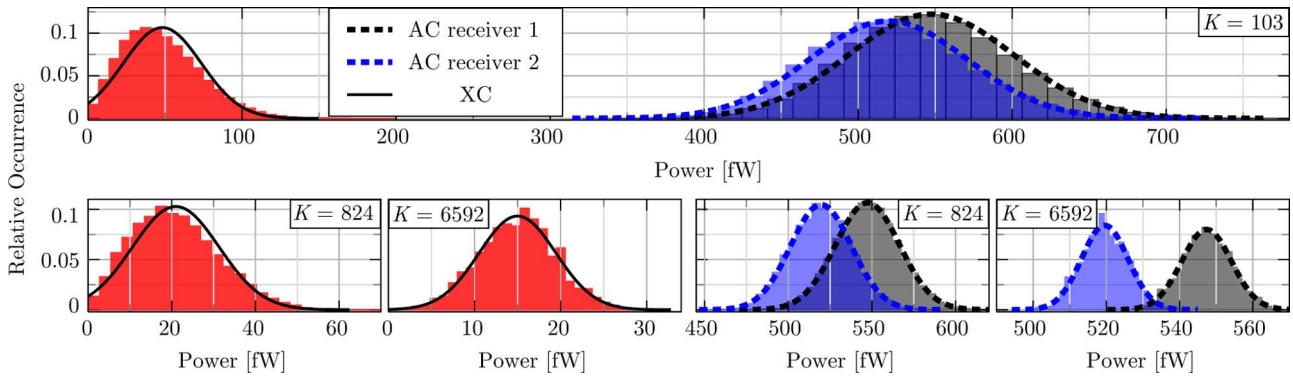

Fig. 9. Distribution of the measured noise power (bins), and Gaussian fits (lines), for several K for XC (left), as well as for the individual receivers (right).

to come from the circuitry itself. In the measurements, they are simply treated as noise.

The noise floor is higher near the band edges due to noise aliasing [visible in Fig. 8(a)]. The difference in the noise floor in the two receivers is caused by loss due to on-chip switches to connect the receivers. The final noise floor obtained using XC is about 15.5 dB lower than that of the individual receivers (see Fig. 7), which corresponds to $\rho \approx 10^{-15.5/10} \approx 0.028$. For receiver 1, $U_{\mathrm{dB}} \approx 0.08\,\mathrm{dB}$ (with $U_{\mathrm{dB}} \triangleq 10\log_{10} U$), and for receiver 2, $U_{\mathrm{dB}} \approx 0.07\,\mathrm{dB}$. The noise uncertainty of the two receivers is approximately equal, as expected. For XC with just one average (not shown), the noise floor is the geometric mean of the spectra of the two individual receivers. Indeed, the measurements show $U_{\mathrm{dB}} \approx 0.08\,\mathrm{dB}$. For the final noise floor of $\mathrm{XC}(K = 1.35 \cdot 10^6)$, $U_{\mathrm{dB}} \approx 0.19\,\mathrm{dB}$. Interestingly, U for long XC is *higher*, which probably means that some of the fluctuations are from an external source (the signal generator or interferers) and are not removed through XC. These results in combination with (13) suggest that the SNR-wall for the individual receivers ($\rho = 1, U_{\mathrm{dB}} \approx 0.07\,\mathrm{dB}$) is around $-18\,\mathrm{dB}$, and for XC ($\rho \approx 0.028, U_{\mathrm{dB}} \approx 0.19\,\mathrm{dB}$) the SNR-wall is expected to be $-29\,\mathrm{dB}$, an improvement of more than 10 dB. This will be experimentally verified later.

Some examples of the measured noise power distribution are given in Fig. 9. As expected, the measured noise power distributions converge to a Gaussian for high K. Higher K reduces the variance, and for XC also the mean.

The threshold λ for given $P_{\mathrm{FA,des}}$ and K is set such that in a $P_{\mathrm{FA,des}}$ fraction of the cases the measured values exceed λ. It could be calculated by combining the NF of the receiver and the statistics in (5) and (11), but using the measured results avoids errors introduced by limitations of the model. The thresholds λ_{ac} and λ_{xc} are determined for $P_{\mathrm{FA}} = 0.1$ (see Fig. 10). The noise fluctuations cause λ to be slightly different for each of the measurements; The maximum of all values is used as the final threshold to "guarantee" $P_{\mathrm{FA}} \leq P_{\mathrm{FA,des}}$.

To mimic a noise-like input signal between 2 MHz and 3 MHz at IF, a signal generator outputs a 64-tone signal with center frequency 402.5 MHz, spaced at 15.6 kHz with random initial phase. The SNR is determined by applying a relatively high input power to make the signal clearly visible in the received spectrum (see Fig. 11). The DC-offset at 0 MHz and

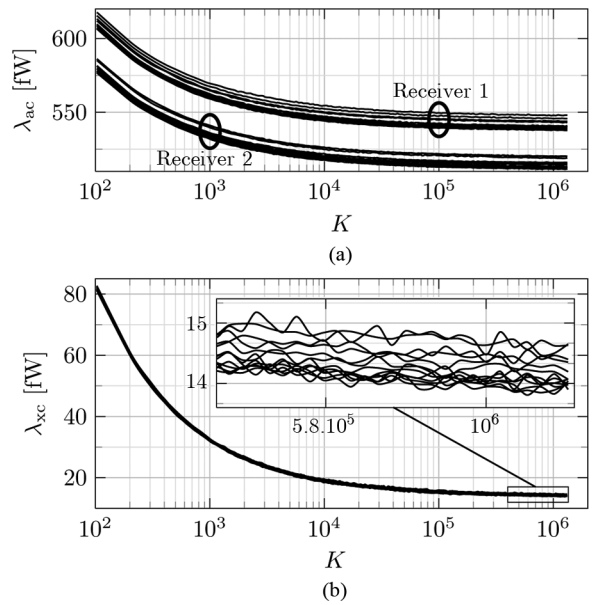

Fig. 10. Obtained thresholds for $P_{\mathrm{FA}} = 0.1$. (a) AC. (b) XC.

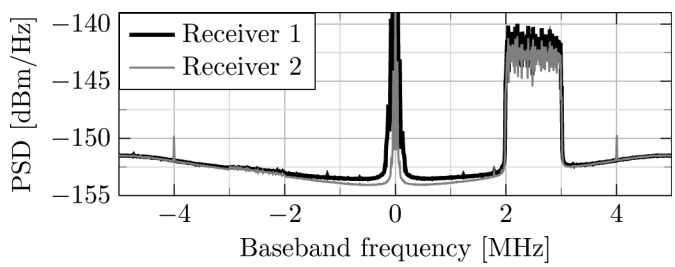

Fig. 11. Output spectrum with a signal present at $\mathrm{SNR} \approx 10$ dB.

the spurs visible at ± 4 MHz in receiver 2 are of no concern as they are outside the band of interest.

With 103 FFT-bins between 2 MHz and 3 MHz, the ADCs capture approximately 103 independent samples in the band of interest per 1024 samples, and K is increased in steps of 103 rather than 1. The total power of the signal is determined by adding the power of the bins between 2 MHz and 3 MHz, and subtracting the average measured power during the noise calibration. With these numbers the SNR turns out to be 10.67 dB

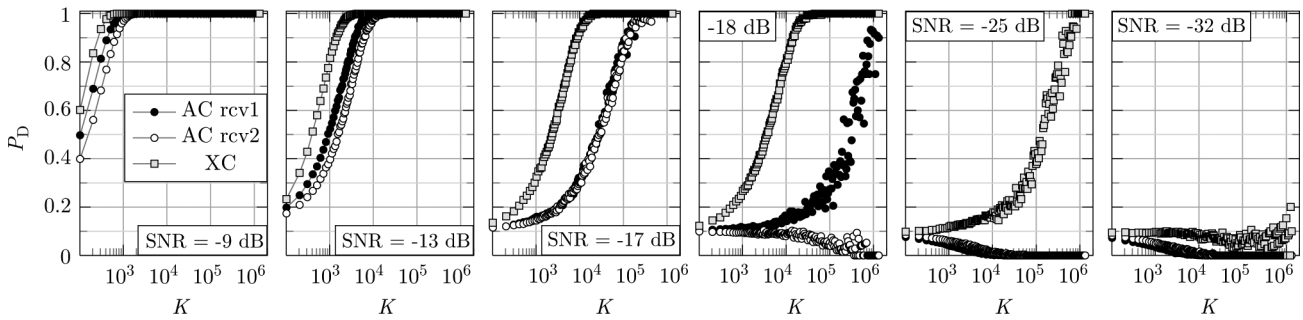

Fig. 12. Measured $P_{\rm D}$ for $P_{\rm FA} = 0.1$ as a function of K in the bandwidth of interest for several SNRs.

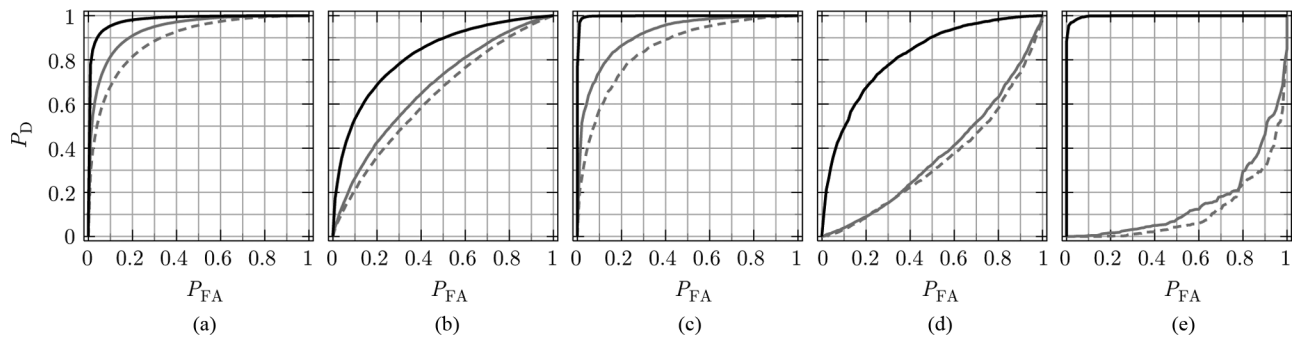

Fig. 13. Measured ROC-curves for several K and SNR, comparing AC of receiver 1 (solid gray) and receiver 2 (dashed gray) to XC (solid black). Note that the SNR of receiver 1 is 0.9 dB higher than the SNR of receiver 2, and the SNR of XC is in between that of the two individual receivers. (a) $\mathrm{SNR}/K = -10\,\mathrm{dB}/515$. (b) $\mathrm{SNR}/K = -15\,\mathrm{dB}/10^3$. (c) $\mathrm{SNR}/K = -15\,\mathrm{dB}/10^4$. (d) $\mathrm{SNR}/K = -20\,\mathrm{dB}/10^4$. (e) $\mathrm{SNR}/K = -20\,\mathrm{dB}/10^5$.

for receiver 1, and 9.77 dB for receiver 2. Regardless of this 0.9 dB difference, it will be referred to as the measurement with $\mathrm{SNR} = 10\,\mathrm{dB}$. Reducing the output power of the signal generator by 1 dB reduces the SNR of each receiver by 1 dB. Smaller FFTs would give more information at higher SNR, but that is of no interest for SNR-wall measurements.

Finally, the input signal is applied, and the threshold values found earlier are used to determine $P_{\rm D}$ for several SNRs. In each measurement, 2^{27} complex samples per receiver are captured (limited by computer memory), which results in 13.5 million independent samples available to detect the signal. To determine $P_{\rm D}$, 10 independent realizations can be considered the minimum required to compare to $P_{\rm MD,des} = 0.1$, leaving maximally 1.35 million samples available.

B. Measurement Results

Fig. 12 shows the measured $P_{\rm D}$ as a function of K in the bandwidth of interest for several SNRs. As expected, $P_{\rm D}$ starts at $P_{\rm FA,des}$, and gradually increases with more samples. The 0.9 dB lower SNR of the second receiver theoretically requires $(10^{0.9/10})^2 \approx 1.5$ times more samples, which is in close agreement with the measurement results. XC clearly obtains the desired $P_{\rm D}$ faster than the individual receivers.

The SNR-wall for AC shows up at $\mathrm{SNR} \approx -18\,\mathrm{dB}$. $P_{\rm D}$ of receiver 2 goes down rather than up, which is a clear sign of an overestimation (biased threshold) of the noise level. With a 0.9 dB higher SNR, $P_{\rm D}$ of receiver 1 still goes to 1. XC is now about two orders of magnitude faster than receiver 1, as predicted in [8]. At $\mathrm{SNR} = -25\,\mathrm{dB}$, $P_{\rm D}$ of both receivers goes to 0, while XC still goes to 1. However, at $\mathrm{SNR} = -32\,\mathrm{dB}$, the $P_{\rm D}$ for XC also stays at or below 0.1.

The receiver operating characteristic (ROC)-curves can also be plotted. These curves explicitly show the trade-off between false alarms and missed detections: allowing a higher $P_{\rm FA}$ increases $P_{\rm D}$. Fig. 13 shows a few representative examples. In principle, the higher the area under the ROC-curve (for the same K and SNR), the better the detector [29].

At $\mathrm{SNR} = -10\,\mathrm{dB}$ [Fig. 13(a)], only a few hundred samples are required to obtain both a satisfactory $P_{\rm FA}$ and $P_{\rm D}$. Fig. 13(b) and (c) show that the detector performance improves when the number of samples increases. The XC-detector clearly outperforms the AC-detectors in all cases. At $\mathrm{SNR} = -20\,\mathrm{dB}$ [Fig. 13(d) and (e)], the ROC-curves of the individual receivers drop below the line $P_{\rm FA} = P_{\rm D}$, which is a key characteristic that this SNR is below the SNR-wall of these receivers. In other words, the area under the ROC-curve can be smaller than $1/2$ in the presence of noise uncertainty, a fact that seems to have been missed by [29].

In Fig. 14, the results are summarized by showing the required number of samples versus SNR to obtain $P_{\rm FA} = 0.1$ and $P_{\rm D} = 0.9$. We explicitly show the number of samples rather than the actual measurement time, because the captured band of 10 MHz can be subdivided in as many bands as desired in the digital domain. The measurement time increases inversely with the resolution: for x Hz of RBW, $1/x$ s of measurement time is required to get 1 independent sample. For this measurement of

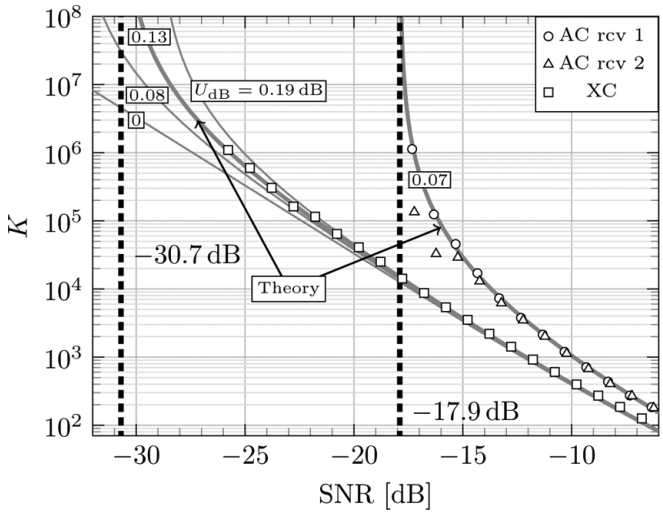

Fig. 14. Sample complexity versus SNR for $P_{\mathrm{FA}} = 0.1$ and $P_{\mathrm{D}} = 0.9$.

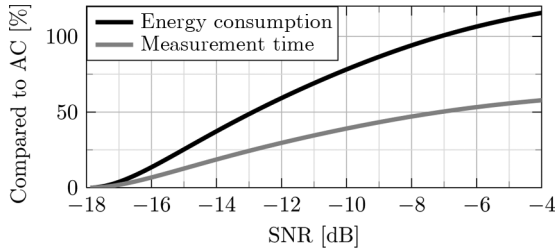

Fig. 15. Measured performance of XC as compared to AC in terms of energy consumption and measurement time as a function of SNR.

1 MHz bandwidth, K can be multiplied by 1 μs to get the measurement time.[3]

Here, the actual SNR for each receiver is used (e.g., -12.33 dB for receiver 1 and -13.23 dB for receiver 2, whereas both are indicated as SNR $= -13$ dB in Fig. 12). To remove false positives, the number of samples is determined as the minimum number of samples required to have $P_{\mathrm{D}} \geq 0.9$ for all measurements with K equal to or larger than this number of samples. This means that at SNR $= -25$ dB, XC needs $6 \cdot 10^5$ samples for $P_{\mathrm{D}} \geq 0.9$ (even though P_{D} was occasionally measured to be above 0.9 for several lower K, see Fig. 12).

The required measurement time can be calculated *a priori* based on the power that needs to be detected and the P_{D} set by regulations, combined with the NF of the receiver and the noise uncertainty. These theoretical curves are shown in Fig. 14 for AC and XC, which are obtained by numerical evaluation from (4) and (11), with $\rho = 0.028$ for XC. $U_{\mathrm{dB}} = 0.13$ dB seems to fit better than $U_{\mathrm{dB}} = 0.08$ dB or $U_{\mathrm{dB}} = 0.19$ dB, although the differences are small. The results clearly show that XC can detect significantly lower signal powers than AC, as predicted in [8]. Based on this $U_{\mathrm{dB}} = 0.13$ dB, an SNR-wall of -30.7 dB is found.

The FCC-requirement of -114 dBm in 6 MHz bandwidth corresponds to -182 dBm/Hz. With a 20 dB receiver NF, the SNR-wall of -30.7 dB for XC results in a maximum sensitivity of -184 dBm/Hz. For -182 dBm/Hz, $SNR = -28$ dB, which requires approximately 10^7 samples (see Fig. 14), equivalent to a measurement time of 1.7 s. In less adverse spectrum conditions, the 10 dB input attenuation may be removed, which reduces the sensing time by approximately a factor 100 to around 17 ms. Note, however, that the noise uncertainty in this well-conditioned setup may be lower than what is feasible in practice (of which the noise uncertainty is estimated to be 1 dB [30]). For 1 dB noise uncertainty, the sensitivity can be calculated to be -175 dBm/Hz, which does not meet the FCC-requirement. Nevertheless, it can still achieve that sensitivity with a linearity of $+25$ dBm IIP3. This is at least 15 dB better than the receivers in Table I if they were to employ AC with 1 dB noise uncertainty at the same sensitivity. As a result, our frontend can withstand at least 15 dB stronger interferers for the same degradation in sensing performance. This comes at the cost of an increase in measurement time, since the input attenuation degrades the SNR.

A fair comparison of the energy efficiency of this spectrum sensing system with others published in the literature requires the analog and digital parts to be fully integrated, both of which is as of yet not the case for published spectrum sensing systems [31]–[33]. Moreover, the measurement conditions should be as similar as possible. Therefore, the measured performance of the XC technique is only compared here to the measured performance of AC using the same system. Fig. 15 shows the measurement time and energy consumption of XC ($U_{\mathrm{dB}} = 0.13$ dB) compared to AC ($U_{\mathrm{dB}} = 0.07$ dB) for the prototype. The energy consumption is measured as the power consumption multiplied with the required measurement time. The power consumption of AC is taken as half the power consumption of XC, since only one receiver is used (rather than two), and the required digital processing is also roughly halved. The measurement time is taken from the theoretical curves in Fig. 14.

For SNRs above -7 dB ($K < 200$, see Fig. 14), AC is more energy-efficient than XC as $\widetilde{P}_{\mathrm{xc}}$ has a higher variance for low K [8]. However, XC takes significantly less measurement time, which reduces the sensing overhead in terms of spectral efficiency, as more time can be spent for data communications. Furthermore, for SNRs below -7 dB, XC is not only more than twice as fast as AC, but also more energy-efficient, as shown in Fig. 15. So XC spectrum sensing can save both on battery life and spectral efficiency.

VI. Conclusion

Spectrum sensing for cognitive radio or dynamic spectrum access requires a high sensitivity and good interferer robustness in order to detect very weak signals in the presence of very strong ones. One approach that works in arbitrary frequency bands is ED, which measures the power in a certain frequency band, and thus does not require any knowledge of the signals to be detected. Unfortunately, it suffers from an SNR-wall due to noise uncertainty: a minimum SNR below which signals cannot be reliably detected.

The standard form of ED is AC. With AC, the power estimate is obtained by squaring and integrating the receiver output.

[3]In theory, the RBW can be made as small as desired, provided enough measurement time is available. However, in practice the LO and sampling clock will have some jitter, which will limit the minimum useful RBW.

Closely related to AC is XC; here the power estimate is obtained by multiplying the outputs of two receivers operating on the same signal. XC was previously proposed to lower the SNR-wall for ED, as well as a means to mitigate several analog impairments on spectrum sensing, such as phase noise of the local oscillator and nonlinearity of the receiver. The linearity can be improved by input attenuation, and the additional noise removed through XC: 3 dB of attenuation gives 3 dB improvement in linearity, and 2 dB improvement in spurious-free dynamic range but costs a factor 4 in measurement time to keep the same sensitivity. Experimental proof on the sensitivity or detection performance, however, was still lacking.

A prototype, designed for high linearity in order to cope with strong signals that may be present in adjacent channels, was implemented in $65\,\mathrm{nm}$ CMOS to provide this experimental proof. By construction, this prototype allows a fair comparison between XC and AC with respect to sensitivity to gain and noise level fluctuations, as the samples for AC and XC can be shared. The prototype shows that, under the measurement conditions detailed in Section V, XC is able to detect signals 30 dB below the noise floor, while AC can only detect signals 18 dB below the noise floor. In other words, XC has a 12 dB lower SNR-wall than AC. As XC requires two receivers and roughly double the amount of digital processing, it has twice the power consumption of AC. This penalty is offset by the fact that XC is significantly faster than AC: at -8 dB SNR and below, XC is more than twice as fast, and therefore more energy-efficient. This not only reduces the spectrum sensing overhead, allowing more time for actual data transmission in dynamic spectrum access, but also makes XC more energy-efficient than AC, prolonging battery life.

ACKNOWLEDGMENT

The authors would like to acknowledge ST for silicon donation, with special thanks to A. Cathelin of ST and S. Dumont of CMP.

REFERENCES

[1] S. K. Jones, T. W. Phillips, H. L. van Tuyl, and R. D. Weller, Evaluation of the performance of prototype TV-band white space devices phase II Office Eng. Technol., Fed. Commun. Commiss., Tech. Rep., Oct. 2008.

[2] In the matter of unlicensed operation in the TV broadcast bands and additional spectrum for unlicensed devices below 900 MHz and in the 3 GHz band FCC, Tech. Rep., Sep. 2010.

[3] D. H. Mahrof, E. A. M. Klumperink, J. C. Haartsen, and B. Nauta, "On the effect of spectral location of interferers on linearity requirements for wideband cognitive radio receivers," in *Proc. 4th IEEE Symp. New Frontiers Dynamic Spectrum Access Netw.*, Singapore, Apr. 6–9, 2010, pp. 1–9.

[4] D. T. Lin, C. Hyungil, L. Li, and M. P. Flynn, "A 600MHz to 3.4 GHz flexible spectrum-sensing receiver with spectrum-adaptive reconfigurable DT filtering," in *Proc. IEEE Radio Frequency Integrat. Circuits Symp.*, Montréal, Canada, Jun. 17–19, 2012, pp. 269–272.

[5] E. A. M. Klumperink, R. Shrestha, E. Mensink, V. J. Arkesteijn, and B. Nauta, "Cognitive radios for dynamic spectrum access—Polyphase multipath radio circuits for dynamic spectrum access," *IEEE Commun. Mag.*, vol. 45, no. 5, pp. 104–112, May 2007.

[6] S. Subhan, E. A. M. Klumperink, and B. Nauta, "Towards suppression of all harmonics in a polyphase multipath transmitter," in *IEEE Int. Symp. Circuits Syst.*, Rio de Janeiro, Brazil, May 15–18, 2011, pp. 2185–2188.

[7] M. S. Oude Alink, E. A. M. Klumperink, M. C. M. Soer, A. B. J. Kokkeler, and B. Nauta, "A 50MHz-to-1.5GHz cross-correlation CMOS spectrum analyzer for cognitive radio with 89dB SFDR in 1MHz RBW," in *Proc. 4th IEEE Symp. New Frontiers Dynamic Spectrum Access Netw.*, Singapore, Apr. 6–9, 2010, pp. 1–6.

[8] M. S. Oude Alink, A. B. J. Kokkeler, E. A. M. Klumperink, G. J. M. Smit, and B. Nauta, "Lowering the SNR wall for energy detection using cross-correlation," *IEEE Trans. Veh. Technol.*, vol. 60, no. 8, pp. 3748–3757, Oct. 2011.

[9] M. S. Oude Alink, E. A. M. Klumperink, A. B. J. Kokkeler, M. C. M. Soer, G. J. M. Smit, and B. Nauta, "A CMOS-compatible spectrum analyzer for cognitive radio exploiting crosscorrelation to improve linearity and noise performance," *IEEE Trans. Circuits Syst. I*, vol. 59, no. 3, pp. 479–492, Mar. 2012.

[10] M. S. Oude Alink, E. A. M. Klumperink, A. B. J. Kokkeler, Z. Ru, W. Cheng, and B. Nauta, "Using crosscorrelation to mitigate analog/RF impairments for integrated spectrum analyzers," *IEEE Trans. Microwave Theory Tech.*, vol. 61, no. 3, pp. 1327–1337, Mar. 2013.

[11] A. Sonnenschein and P. M. Fishman, "Radiometric detection of spread-spectrum signals in noise of uncertain power," *IEEE Trans. Aerosp. Electron. Syst.*, vol. 28, no. 3, pp. 654–660, 1992.

[12] D. B. Čabrić, "Cognitive radios: System design perspective," Ph.D. dissertation, Univ. California, Berkeley, 2007.

[13] R. Tandra and A. Sahai, "SNR walls for signal detection," *IEEE J. Sel. Topics Signal Process.*, vol. 2, no. 1, pp. 4–17, Feb. 2008.

[14] R. Balamurthi, H. Joshi, C. Nguyen, A. Sadek, S. Shellhammer, and C. Shen, "A TV white space spectrum sensing prototype," in *Proc. 5th IEEE Symp. New Frontiers Dynamic Spectrum Access Netw.*, Aachen, Germany, May 3–6, 2011, pp. 297–307.

[15] Shared spectrum company, spectrum occupancy measurements location 4 of 6: Republican National Convention, New York City, New York, August 30, 2004–September 3, 2004, rev. 2, Shared Spectrum Company, Tech. Rep., 2005.

[16] M. C. M. Soer, E. A. M. Klumperink, Z. Ru, F. E. van Vliet, and B. Nauta, "A 0.2-to-2.0GHz 65nm CMOS receiver without LNA achieving $>$ 11 dBm IIP3 and $<$ 6.5 dB NF," in *Proc. IEEE Int. Solid-State Circuits Conf.— Dig. Tech. Papers*, San Francisco, CA, Feb. 8–12, 2009, pp. 222–223,223a.

[17] Z. Ru, N. Moseley, E. Klumperink, and B. Nauta, "Digitally enhanced software-defined radio receiver robust to out-of-band interference," *IEEE J. Solid-State Circuits*, vol. 44, no. 12, pp. 3359–3375, Dec. 2009.

[18] L. Cai and R. Harjani, "1–10GHz inductorless receiver in $0.13\mu\mathrm{m}$ CMOS," in *Proc. IEEE Radio Freq. Integrat. Circuits Symp.*, Boston, MA, Jun. 7–9, 2009, p. 61.

[19] S. Blaakmeer, E. Klumperink, D. Leenaerts, and B. Nauta, "The blixer, a wideband balun-LNA-I/Q-mixer topology," *IEEE J. Solid-State Circuits*, vol. 43, no. 12, pp. 2706–2715, Dec. 2008.

[20] D. Leenaerts, R. van de Beek, J. Bergervoet, H. Kundur, G. van de Weide, A. Kapoor, T. Y. Pu, Y. Fang, Y. J. Wang, B. J. Mukkada, H. S. Lim, M. Kiran, C. S. Lim, S. Badiu, and A. Chang, "A 65nm CMOS inductorless triple-band-group wimedia UWB PHY," in *Proc. IEEE Int. Solid-State Circuits Conf.—Dig. Tech. Papers*, San Francisco, CA, Feb. 8–12, 2009, pp. 410–411,411a.

[21] J. Greenberg, F. D. Bernardinis, C. Tinella, A. Milani, J. Pan, P. Uggetti, M. Sosio, S. Dai, S. Tang, G. Cesura, G. Gandolfi, V. Colonna, and R. Castello, "A 40MHz-to-1GHz fully integrated multi-standard silicon tuner in 80nm CMOS," in *Proc. IEEE Int. Solid-State Circuits Conf.—Dig. Tech. Papers*, San Francisco, CA, Feb. 19–23, 2012, pp. 162–164.

[22] D. Murphy, H. Darabi, A. Abidi, A. A. Hafez, A. Mirzaei, M. Mikhemar, and M. -C. F. Chang, "A blocker-tolerant, noise-cancelling receiver suitable for wideband wireless applications," *IEEE J. Solid-State Circuits*, vol. 47, no. 12, pp. 2943–2963, Dec. 2012.

[23] S. Youssef, R. van de Zee, and B. Nauta, "Active feedback technique for RF channel selection in front-end receivers," *IEEE J. Solid-State Circuits*, vol. 47, no. 12, pp. 3130–3144, Dec. 2012.

[24] T. H. Lee, *The Design of CMOS Radio-Frequency Integrated Circuits*. Cambridge, U.K.: Cambridge Univ. Press, 2004.

[25] C. Rauscher, *Fundamentals of Spectrum Analysis*, 1 ed. Munich, Germany: Rohde Schwarz, 2001.

[26] W. Cheng, M. S. Oude Alink, A. J. Annema, G. J. M. Wienk, and B. Nauta, "A wideband IM3 cancellation technique for CMOS Π and T-attenuators," *IEEE J. Solid-State Circuits*, vol. 48, no. 2, pp. 358–368, Feb. 2013.

[27] M. S. Oude Alink, A. B. J. Kokkeler, E. A. M. Klumperink, Z. Ru, W. Cheng, and B. Nauta, "Improving harmonic rejection for spectrum sensing using crosscorrelation," in *Proc. European Solid-State Circuits Conf.*, Bordeaux, France, Sep. 17–21, 2012, pp. 361–364.
[28] M. S. Oude Alink, "RF spectrum sensing in CMOS exploiting cross-correlation," Ph.D. dissertation, Univ. Twente, Enschede, The Netherlands, 2013.
[29] S. Atapattu, C. Tellambura, and H. Jiang, "Analysis of area under the ROC curve of energy detection," *IEEE Trans. Wireless Commun.*, vol. 9, no. 3, pp. 1216–1225, Mar. 2010.
[30] S. Shellhammer and R. Tandra, Performance of the power detector with noise uncertainty. Jul. 2006 [Online]. Available: http://www.ieee802.org/22/Meeting_documents/2006_July/22-06-0134-00-0000_Performance-of-the-power-detector-with-Noise-Uncertainty.ppt
[31] J. Park, T. Song, J. Hur, S. M. Lee, J. Choi, K. Kim, K. Lim, C. -H. Lee, H. Kim, and J. Laskar, "A fully integrated UHF-band CMOS receiver with multi-resolution spectrum sensing (MRSS) functionality for IEEE 802.22 cognitive radio applications," *IEEE J. Solid-State Circuits*, vol. 44, no. 1, pp. 258–268, Jan. 2009.
[32] M. Kitsunezuka, H. Kodama, N. Oshima, K. Kunihiro, T. Maeda, and M. Fukaishi, "A 30-MHz-2.4-GHz CMOS receiver with integrated RF filter and dynamic-range-scalable energy detector for cognitive radio systems," *IEEE J. Solid-State Circuits*, vol. 47, no. 5, pp. 1084–1093, May 2012.
[33] T. -H. Yu, C. -H. Yang, D. Čabrić, and D. Markovic, "A 7.4-mW 200-MS/s wideband spectrum sensing digital baseband processor for cognitive radios," *IEEE J. Solid-State Circuits*, vol. 47, no. 9, pp. 2235–2245, Sep. 2012.

Mark S. Oude Alink (S'09) was born in 1984, Hengelo, The Netherlands. He received the B.Sc. degree in computer science and the M.Sc. degrees in electrical engineering and computer science, and the Ph.D. degree (all *cum laude*), all from the University of Twente, Enschede, The Netherlands, in 2004, 2008, and 2013, respectively.

He currently works as a System Engineer and IC-designer at Bruco Integrated Circuits, Borne, The Netherlands.

André B. J. Kokkeler received the Ph.D. degree on the thesis "Analog-digital Codesign using Coarse Quantization," from the University of Twente, Enschede, The Netherlands, in 2005.

He has worked more than six years at Ericsson as a System Engineer and eight years at The Netherlands Foundation for Research in Astronomy (ASTRON) as a Scientific Project Manager. In 2003, he joined the University of Twente, Twente, The Netherlands. He has a background in telecommunication, mixed-signal design, and signal processing. Currently, his main interest lies in the area of applying low-power design techniques for computationally intensive applications. The emphasis is on reconfigurable architectures for streaming applications. He is involved in research projects, sponsored by the Dutch and European governments and industry.

Eric A. M. Klumperink (M'98–SM'06) was born on April 4, 1960, in Lichtenvoorde, The Netherlands. He received the B.Sc. degree from HTS, Enschede, The Netherlands, in 1982, and the Ph.D. degree from University of Twente, Enschede, The Netherlands, in 1997.

After a short period in industry, he joined the Faculty of Electrical Engineering of the University of Twente (UT), Enschede, The Netherlands, in 1984, participating in analog CMOS circuit design and research. This resulted in several publications and a Ph.D. thesis "Transconductance based CMOS circuits". After receiving the Ph.D. degree, he started working on RF CMOS circuits. He is currently an Associate Professor at the IC-Design Laboratory which participates in the CTIT Research Institute at UT. He holds several patents and has authored or coauthored more than 80 journal and conference papers.

Dr. Klumperink served as an Associate Editor for IEEE TRANSACTIONS ON CIRCUITS AND SYSTEMS II in 2006 and 2007, and for IEEE TRANSACTIONS ON CIRCUITS AND SYSTEMS I since 2008. He was a corecipient of the ISSCC 2002 Van Vessem Outstanding Paper Award.

Gerard J. M. Smit received the M.Sc. degree in electrical engineering from the University of Twente, Enschede, The Netherlands. He finished the Ph.D. thesis entitled "The design of central switch communication systems for multimedia applications," from the same university in 1994.

He currently is a Full Professor with the faculty of EEMCS, University of Twente, leading the CAES Chair, where he is responsible for a number of research projects sponsored by the EC, industry and Dutch government in the field of multimedia and efficient reconfigurable systems. After receiving the M.Sc. degree, he worked for four years at the Research laboratory of Océ, Venlo, The Netherlands. In 1994, he was a Visiting Researcher with the Computer Laboratory, Cambridge University, Cambridge, U.K., and, in 1998, he was a Visiting Researcher with Lucent Technologies Bell Labs Innovations, Murray Hill, NJ, USA. Since 1999, he has been leading the Chameleon group, which investigates new hardware and software architectures for energy-efficient systems. Currently his research interests include low-power communication, and reconfigurable architectures for energy reduction.

Bram Nauta (M'91–SM'03–F'08) was born in Hengelo, The Netherlands, in 1964. He received the M.Sc. degree (*cum laude*) in electrical engineering and the Ph.D. degree on the subject of analog CMOS filters for very high frequencies from the University of Twente, Enschede, The Netherlands, in 1987 and 1991, respectively.

In 1991, he joined the Mixed-Signal Circuits and Systems Department of Philips Research, Eindhoven, The Netherlands, where he worked on high-speed A/D converters and analog key modules. In 1998, he returned to the University of Twente as a full Professor heading the IC Design group, which is part of the CTIT Research Institute. His current research interest is high-speed analog CMOS circuits. He is also a part-time consultant in industry. In 2001, he cofounded Chip Design Works. His Ph.D. degree thesis was published as a book: *Analog CMOS Filters for Very High Frequencies* (Springer, 1993).

Dr. Nauta served as an Associate Editor of IEEE TRANSACTIONS ON CIRCUITS AND SYSTEMS—PART II: ANALOG AND DIGITAL SIGNAL PROCESSING from 1997 to 1999. After this, he served as a Guest Editor, an Associate Editor (2001–2006), and from 2007 as Editor-in-Chief for the IEEE JOURNAL OF SOLID-STATE CIRCUITS. He is also a member of the technical program committees of the IEEE International Solid-State Circuits Conference (ISSCC), the European Solid-State Circuit Conference (ESSCIRC), and the Symposium on VLSI Circuits. He was a corecipient of the ISSCC 2002 Van Vessem Outstanding Paper Award. He received the Shell Study Tour Award for his Ph.D. degree work. He was a distinguished lecturer of the IEEE and is elected member of IEEE SSCS AdCom.